World Academy of Science, Engineering and Technology
International Journal of Electrical and Computer Engineering
Vol:13, No:5, 2019

Performance Assessment of a Variable-Flux Permanent-Magnet Memory Motor

Michel Han, Christophe Besson, Alain Savary, Yvan Becher

***Abstract*—**The variable flux permanent magnet synchronous motor (VF-PMSM), also called "Memory Motor", is a new generation of motor capable of modifying the magnetization state with short pulses of current during operation or standstill. The impact of such operation is the expansion of the operating range in the torque-speed characteristic and an improvement in energy efficiency at high-speed in comparison to conventional permanent magnet synchronous machines (PMSMs). This paper reviews the operating principle and the unique features of the proposed memory motor. The benefits of this concept are highlighted by comparing the performance of the rotor of the VF-PMSM to that of two PM rotors that are typically found in the industry. The investigation emphasizes the properties of the variable magnetization and presents the comparison of the torque-speed characteristic with the capability of loss reduction in a VF-PMSM by means of experimental results, especially when tests are conducted under identical conditions for each rotor (same stator, same inverter and same experimental setup). The experimental results demonstrated that the VF-PMSM gives an additional degree of freedom to optimize the efficiency over a wide speed range. Thus, with a design easy to manufacture and with the possibility of controlling the magnetization and the demagnetization of the magnets during operations, the VF-PMSM can be interesting for various applications.

***Keywords*—**Efficiency, magnetization state, memory motors, performances, permanent-magnet, synchronous machine, variable-flux, variable magnetization, wide speed application

I. Introduction

PMSMs are widely used in many applications for their high torque density with great efficiency. However, the constant excitation flux generated by the magnets involves a limited speed range. This range is often extended by a flux weakening control, which uses a sustainable armature current to temporarily weaken the flux. Improving performance, flexibility and optimizing the motor efficiency against the operating range are fields of interest in many studies with different solutions [1]-[3]. Some exploited an AC armature winding to control the magnetization state, and others preferred a solution with an additional DC exciter field winding. The use of an exciter field winding allows the control of the excitation flux and gives the desired operating flexibility. However, this excitation winding adds complexity to the system, including an extra inverter.

This project, sponsored by the Swiss Federal Office of Energy (SFOE), was carried out by the University of Applied Sciences Western Switzerland (HES-SO), Yverdon-les-Bains.

Michel Han, Christophe Besson, Alain Savary and Yvan Becher are with the University of Applied Sciences of Western Switzerland, 1400 Yverdon-les-bains, Switzerland (e-mail: michel.han@heig-vd.ch, christophe.besson@heig-vd.ch, alain.savary@heig-vd.ch, yvan.becher@heig-vd.ch).

The approach of the VF-PMSM was proposed to combine the performances of a PMSM with the controllability of flux without any excitation winding [4]. The change of flux intensity crossing the air gap is carried out by means of short pulses of armature current, which modify the magnetization state (MS) of low coercive force magnets. As a result, this method leads to an additional degree of freedom compared to PMSMs and exhibits significant feasibility for a wide range of operating speeds, e.g. machine tools, robotics, and tractions (automobile, railway and E-bike).

MS manipulation requires a high field created from the armature current, which circulates through the magnets. An inverter with proper voltages and currents is necessary in order to provide proper pulses. An eventual extra cost can be justified by the increase in performance.

Different designs have recently been emerging. Some designs propose a memory motor with the NdFeB (Neodymium-Iron-Boron) and the AlNiCo (Aluminium-Nickel-Cobalt) magnets [5]-[8]. Another combination can be made using ferrite magnets [9] to replace the AlNiCo. The effect of magnet series or parallel configuration on a salient pole VF-PMSM was investigated [10]. An alternative design is to only consider low H_c magnets that are usually associated with flux barriers [11]-[13]. Memory motors with an outer rotor have also been designed and show the same flexibility in the wide range speed applications [14], [15].

This paper compares the measured performance of a VF-PMSM with two conventional PM motors, regarding their torque-speed characteristics and efficiency in the optimal torque and flux-weakening domain of operations. All the rotors, as depicted in Fig. 1, are placed in the same typical stator to ensure a fair comparison.

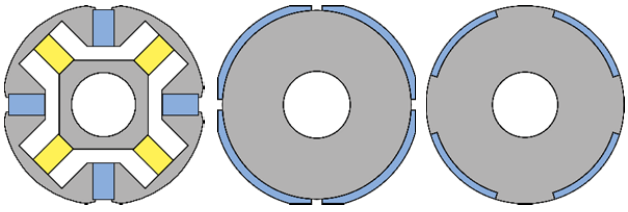

(a) (b) (c)

Fig. 1 Rotor's topologies: (a) VF-PMSM; (b) PMSM-M; (c) PMSM-W

The operating principle of the VF-PMSM, specifically designed for the comparison, is introduced in section II in order to emphasize its unique features. The prototype is briefly described in Section III. Section IV gives special attention to

the prototype's measured performances as well as the losses at different magnetization states. The advantages of the VF-PMSM are highlighted in Section V. In this section, the performance of PM motors is compared with a surface-mounted magnets rotor (M-type) and a surface-inset permanent magnets rotor (W-type) suited, respectively, for high torque applications and operating regimes of flux weakening. Sections VI and VII yield a summary and the conclusion based on this research.

II. Operating Principle

The memory motor presented in this paper uses AlNiCo magnets to adjust its operating points by changing the magnetization level remotely, thus magnets' excitation flux, by means of current pulse while the motor is running. AlNiCo has a low coercive force (50 to 100 kA/m) with a high knee in the B-H characteristic, which allows the change of its magnets operating point without a prohibitive current pulse.

Fig. 2 schematically shows the four-pole rotor of the developed and tested prototype. The rotor has 4 "variable magnetization" AlNiCo magnets allocated in the d-axis and 4 NdFeB magnets in the q-axis with "constant magnetization" clamped by ferromagnetic steels, which help to channel the field. Paramagnetic sections keep all the mechanical parts together. NdFeB magnets have a linear B(H) characteristic over a wide temperature range (and a coercive force up to 20 times higher than AlNiCo), which prevents the NdFeB from being demagnetized, and generates a constant magnetic field that is added to the contribution of AlNiCo. This combination enables a weakening, or an enhancement of the excitation flux provided by the rotor.

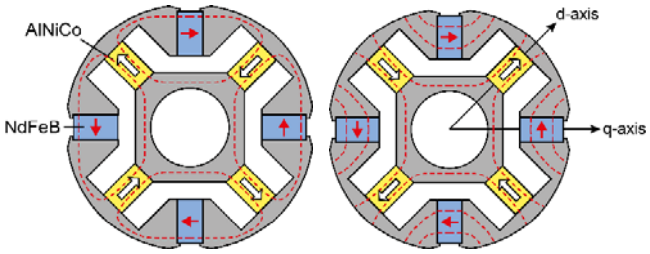

Fig. 2 Orientation of AlNiCo magnets according to the operating modes

As a conventional PM motor, the torque of VF-PMSM is generated by the quadrature component of the armature current, i_q and the component of the direct axis, i_d, acts on the magnets' excitation flux. However, in the case of VF-PMSM, i_d is used as short current pulses of a few tens of milliseconds to change the rotor MS according to load conditions. This allows the torque and the rotor MS to be controlled independently.

The excitation flux will remain unchanged as long as one does not change the magnets' operating point by another current pulse, which explains the alternative denomination "Memory Motor".

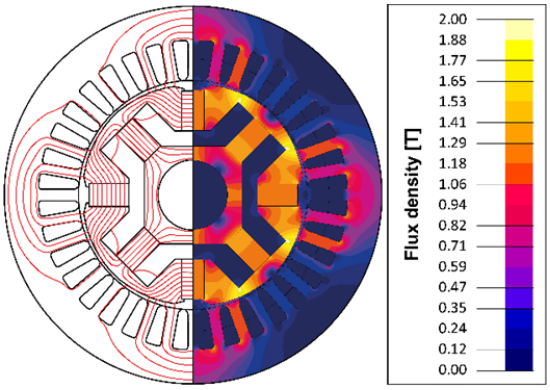

Fig. 3 Open-circuit field distribution and flux density when excitation flux is minimum (min MS)

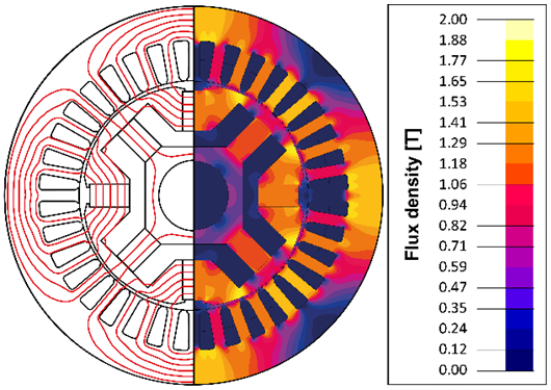

Fig. 4 Open-circuit field distribution and flux density when excitation flux is maximum (max MS)

The orientation of AlNiCo involves a different field distribution within the rotor and the flux crossing the air gap, as depicted in Figs. 3 and in Fig. 4.

Fig. 3 shows the field distribution when the rotor magnetization state is minimum (min MS). The field created by the AlNiCo flows in the same direction as the one from NdFeB. The resulting field circulating through the air gap is minimum since it is mostly flowing within the rotor. The induced voltage constant also called the back-emf constant is therefore small. The motor is well-suited for working at high speed and low torque (HS-LT).

By applying current pulses, the polarization of AlNiCo can be reversed. In this case, the fields' interaction between AlNiCo and NdFeB results in a distribution as seen in Fig. 4. The magnetization state of the rotor is therefore maximum (max MS) and so is the flux circulating in the stator coil. With a high torque constant, the motor becomes well-suited for working at low speed and high torque (LS-HT).

Thus, according to the orientation of AlNiCo magnets, it is possible to provide a motor with two operating modes:

1. High speed and low torque (HS-LT, left in Fig. 2)
2. Low speed and high torque (LS-HT, right in Fig. 2)

There are numerous applications (machine tools, robotics, etc.) where two torque-speed characteristics are required. These types of operations are well-suited for laundry machines that have both washing and draining modes, which need

respectively a LS-HT and a HS-LT operation. Or, for two-speed applications such as actuators for robotics, where the motor must be able to bear large loads while operating slowly, and also to operate quickly with almost no load.

The polarity change of AlNiCo magnets can be carried out when the motor is stopped for a brief instant to apply the current pulse before its use. Note that these two modes are only considered in this section for the sake of clarity in the explanation. It is clear that intermediate rotor MS can be reached by acting on the amplitude and duration of applied current pulses, to adjust the magnets' excitation flux. Furthermore, pulse i_d can be applied to change the modes during operations. In such case, gradually magnetizing or demagnetizing the magnets may avoid any harmful transient effects.

TABLE I
PARAMETERS OF VF-PMSM

Symbol	Quantity	Unit	Value
P_n	Rated Power	kW	1.6
T_n	Rated Torque	Nm	9
Ω_n	Rated Speed	rpm	1700
Ω_{max}	Maximum Speed	rpm	3720
$Ø_{stat}$	Stator diameter	mm	170
m	Number of phases	-	3
p	Number of poles pairs	-	2
I_n	Rated Current	A_{rms}	3
V_{DC}	DC bus voltage	V	600

III. PROTOTYPE OF VF-PMSM

Sizing a VF-PMSM is a complex task that must meet specific requirements as well as take into account the strong non-linear B-H characteristic of AlNiCo, and the saturation effects. Criteria that are subject to special attention include:

1. Sizing must consider the capability of changing the rotor MS with an amplitude of i_d pulses, usually from 5 to 7 pu, which is acceptable from a conventional inverter.
2. During the absence of pulses, the magnetization level of AlNiCo must not be changed by i_q, typically 4 to 5 pu in a transient phase to produce a peak torque.
3. The material, the dimensions of NdFeB magnets and the dimensions of the rotor's bridges must be carefully designed in order to prevent any irreversible demagnetization of NdFeB ("constant magnetization").

In numerous applications with a motion profile that require fast accelerations (machine tools or robotics), peak torques require transient current of about 3 to 7 times the rated current. The converter is thus selected based on these peak currents and not only on the basis of the rated current of the motor. For a VF-PMSM, the amplitude of i_d current pulse does not lead to a costly oversize of the converter. Furthermore, it is worth noting that the short duration of the i_d pulses allows taking advantage of the thermal constant of the IGBT's, used in the inverter. This avoids any temperature increase of the inverter during the application of the pulses.

The presented prototype is shown in Fig. 5, and its specifications are reported in Table I. The considered stator, made of stacked sheets (IEC 112/4.103, M600-50A) without skewing, has a distributed winding to generate a magneto motive force with low spatial harmonics. Widely found among manufacturers, this stator was purposely selected to demonstrate the operation feasibility of VF-PMSM without any specific equipment. The rotor was optimized using finite element analysis with the software Flux2D. The external shape of the rotor with an uneven air gap leads to a simulated torque ripple that is close to 8% for the nominal conditions.

(a) (b)

Fig. 5 (a) Rotor of VF-PMSM; (b) 36-slots stator

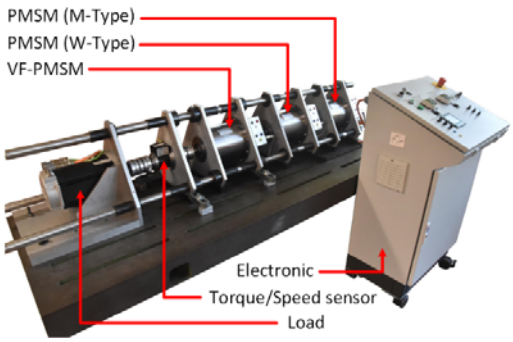

Fig. 6 Experimental set-up

IV. CHARACTERISTICS OF VF-PMSM

The measurements come from the experimental set-up seen in Fig. 6. Different sensors provide data of electrical and mechanical quantities such as current, voltage, electric power, position, speed, torque and mechanical power. A graphical interface developed with LabView software identifies and displays measurement data to visualize their instantaneous values.

A field-oriented vector control is implemented in a microcontroller to control a conventional 3-phase half bridge inverter. This strategy is commonly used for PMSM in the industry, where speed is regulated via the component i_q related to the torque, by means of some cascaded controllers. The current i_d is usually set at zero, unless a flux weakening is required. For the case with the VF-PMSM, the use of i_d enables a current pulse to switch the operating modes, as described in Section II.

A. Motor Constants

The rotating field created by the permanent magnets induces a voltage in the phase coils. This induced voltage is derived directly from the excitation flux waveform by Faraday's Law. Since RMS-value of the back-emf voltage

V_{emf} is proportional to the speed Ω, in practice, the back-emf constant K_E is defined as

$$\begin{cases} V_{emf} = K_E \cdot \Omega \\ K_E = \frac{1}{\sqrt{2}} k_w \, p \, N \, \phi_E \end{cases} \quad (1)$$

where K_E is in $V_{ph\text{-}rms}$·s/rad, p is the number of pole pairs, Ω is the speed in (rad/s), k_w is the winding factor, N is the total number of turns in series per phase, and Φ_E is the fundamental flux per pole due to the magnets. When the set of equations (1), are combined together, the result is

$$V_{emf} = \frac{1}{\sqrt{2}} k_w \, p \, N \, \phi_E \Omega \quad (2)$$

Equation (2) illustrates the proportionality between the induced voltage and the excitation flux, which means the amplitude of back-emf is a direct indication of magnetization level assuming the speed is constant.

Fig. 7 shows the back-emf measured in the cases of max MS and min MS with the ones from the simulations, which show good agreements and validate the FE simulation model developed for the prototype. The voltage constants were estimated to be 0.535 V_{rms}/rad/s and 1.109 V_{rms}/rad/s when the rotor MS is minimum ($K_{E,min}$) or maximum ($K_{E,max}$), respectively. Furthermore, their ratio denotes that the back-emf constant can be controlled by a factor 2.07.

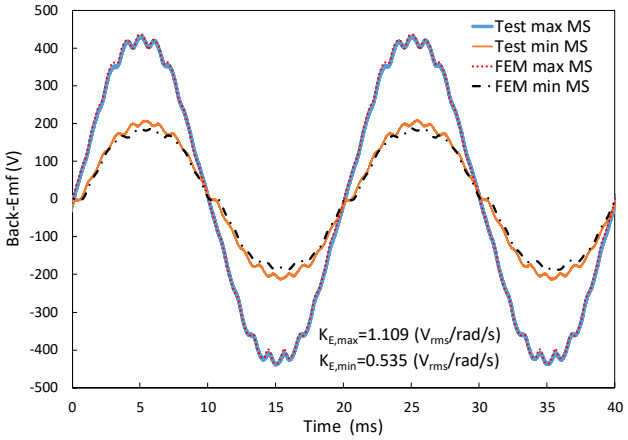

Fig. 7 Measured phase-to-phase no-load voltage at 1500 rpm

Fig. 8 shows the characteristics of magnetization and demagnetization, represented through the induced voltages against the current i_d. These characteristics permit the estimation of the rotor MS when a pulse of i_d is applied. The min and max MS are reached with a pulse of 6.5 pu. It also presents an asymmetry in the magnetization and demagnetization process. Indeed, the magnetization process requires a current i_d of 6.5 pu to oppose the magnetic field of NdFeB, in addition to the AlNiCo. In the demagnetization process, only a pulse of 4 pu is needed to reach the min MS, thanks to the opposition of fields between the NdFeB and AlNiCo. In the absence of magnetic saturation, the electromagnetic torque Tem is proportional to the armature current I, such as

$$\begin{cases} T_{em} = K_T \cdot I \\ K_T = 3 \, K_E \end{cases} \quad (3)$$

where K_T is the torque constant in Nm/A_{rms}. The parameters, K_E and K_T, directly depend on the rotor MS and can be adapted according to the load.

Fig. 9 presents the characteristic of torque-current for the cases min MS and max MS. The ratios between the measured torque constants, $K_{T,min}$=1.48 Nm/A_{rms} and $K_{T,max}$=3.07 Nm/A_{rms}, are 2.07, as expected. A magnetic saturation appears for high current values. Thus, the test indicates that the VF-PMSM can generate a peak torque in a transient since the rotor MS remains unchanged for i_q up to 4 pu.

Many applications require a motion profile with fast accelerations in a short period of time. During these phases, peak torques are generated, hence the importance of keeping the rotor MS in such transients.

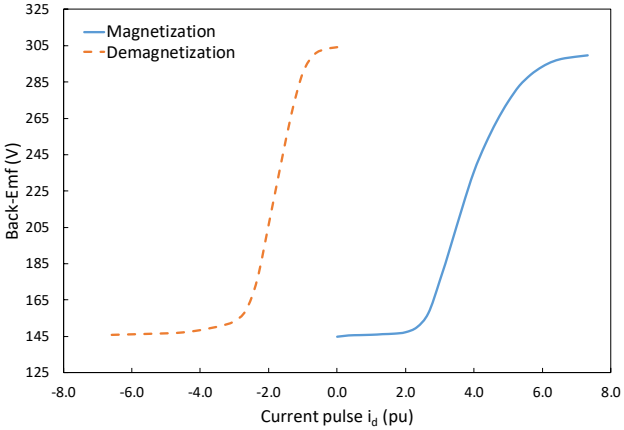

Fig. 8 Measured magnetization and demagnetization characteristic of VF-PMSM at 1500 rpm

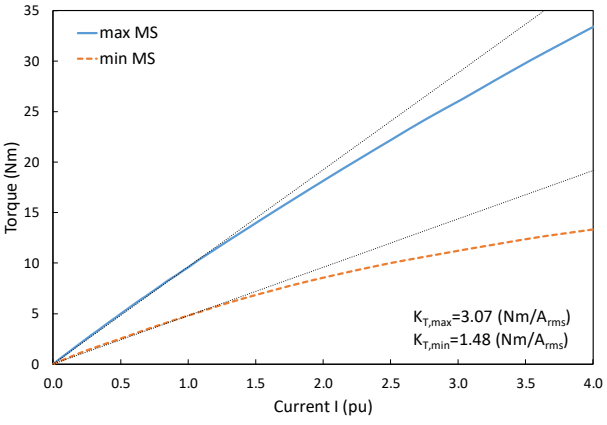

Fig. 9 Measured torque vs current characteristic

B. Typical Example of Current Pulse

Fig.10 shows a typical behaviour during a demagnetization process. A pulse of 2.5 pu is applied for 50 ms on the VF-PMSM running at 500 rpm with a constant load. With a

current initially measured at 1 A_{rms}, the pulse has reduced the magnets' excitation flux. This involves an increase of current, stabilized at 1.65 A_{rms}, in order to provide the same torque, assuming the load and speed are constant.

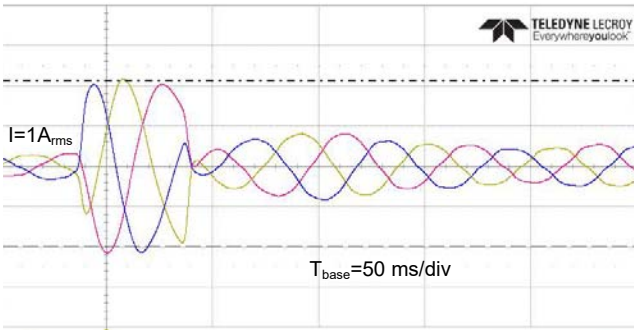

Fig. 10 Transient stator currents in demagnetization process

In addition, the required energy to change the magnetization state was estimated thanks to an experiment. The test consisted of applying a trapezoidal shape pulse of 6.5 pu for 50 ms on the standstill VF-PMSM motor. The 3-phase voltage and the currents were measured using an oscilloscope.

This energy does not include any mechanical losses since the pulse is applied on a standstill memory motor. It is thereby converted into a duration that is equivalent to an amount of time (t_{eq}) when the VF-PMSM is dissipating all the losses (P_{losses}=178W) in nominal operation, as reported in Table II. A pulse represents therefore a negligible energy cost, i.e. the total dissipated losses for less than one second in steady-state nominal operation. However, these losses induced by the pulses can become significant when they are frequently applied [16].

TABLE II
ENERGY CONSUMED IN THE MAGNETIZATION PROCESS WITH A PULSE (I=6.5PU) OF 50 MS

	E (J)	t_{eq} (s)
Pulse of 50 ms	121.1	0.7

C. VF-PMSM Performance

The performance test measures the steady-state torque for the nominal value of i_q, and the motor efficiency at different speeds, where i_d is nil during the operation. This test was carried out for different magnetization levels, modified at standstill, resulting in the characteristics in Fig. 11.

Fig. 12 shows the efficiency of the torque-speed characteristic, measured and plotted in Fig.11, for each considered MS. These measurements show that for each rotor MS, the VF-PMSM has different torque-speed characteristics without the use of flux weakening, which leads to deducing that the memory motor is a fusion of several motors into one.

The combination of all optimum operating points results in an expansion of potential operating range, with a significant increase of efficiency at HS-LT operating mode, represented by a dotted envelope in Figs.11 and 12.

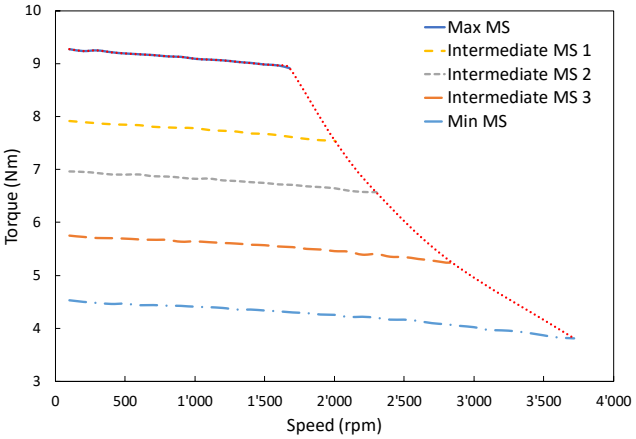

Fig. 11 Measured torque-speed characteristics under nominal current for different magnetization states (I_d=0, I_q =I, V_{DC} = 600 V)

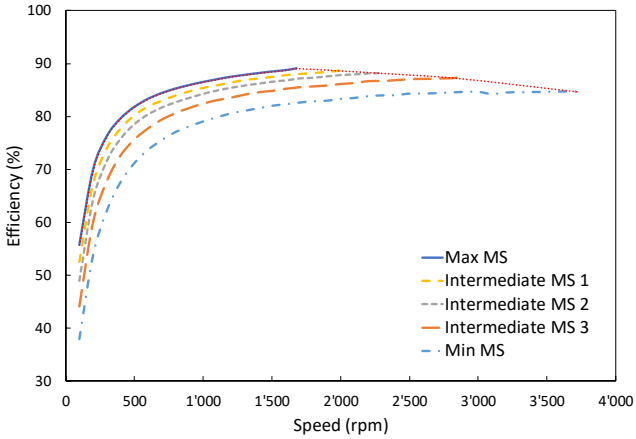

Fig. 12 Measured motor efficiency for different magnetization states

Table III compares the values of VF-PMSM power balances in steady state, measured with a mechanical power of 1500 W and I= i_q. The measured operating points are indicative of the cases with min MS and max MS for the same mechanical power. It is interesting to observe that iron losses stayed relatively low for the high speed, while friction losses increased significantly. For the min MS, the flux density in the stator lamination stack is rather low (Fig. 3) leading to a reduction of the iron losses under high speed conditions. The eddy current losses in the permanent magnets are negligible in the considered speed range of operation.

TABLE III
LOSSES ESTIMATION FOR P_{mec}=1500 (W) IN 2 OPERATING MODES WITH I_q=I_n AND I_d=0 (A)

	Max MS	Min MS
P_{el} (W)	1678	1725
P_{copper} (W)	71	71
P_{iron} (W)	84	74
P_{fric} (W)	23	80
Efficiency (%)	89.4	87.0
Ω (rpm)	1566	3583
T (Nm)	9.15	4

A high rotor MS level is preferred for LS-HT conditions to minimize the copper losses needed to produce the torque, whereas a low rotor MS is preferred for HS-LT conditions to minimize iron losses. The control of the rotor MS can be used to minimizes losses in the operating points of the torque-speed characteristics.

V. Comparison of Performances with Conventional PMSMs

The comparative approach evaluates the performances provided by the three rotors depicted in Fig. 1. Each motor has identical mechanical air gap length of 0.8 mm and is used with the same stator as in Fig. 5. They all provide a nominal mechanical power close to 1.6 kW at different rated speeds.

Fig. 13 represents the torque-speed characteristics with the nominal current I=3 A_{rms}. The torque measured at 1000 rpm for the three motors are 9.92 Nm (M-type), 8.47 Nm (W-type) and 9.30 Nm (VF-PMSM). Note that the VF-PMSM was purposely designed to fit its characteristic between the two PM motors' in LS-HT.

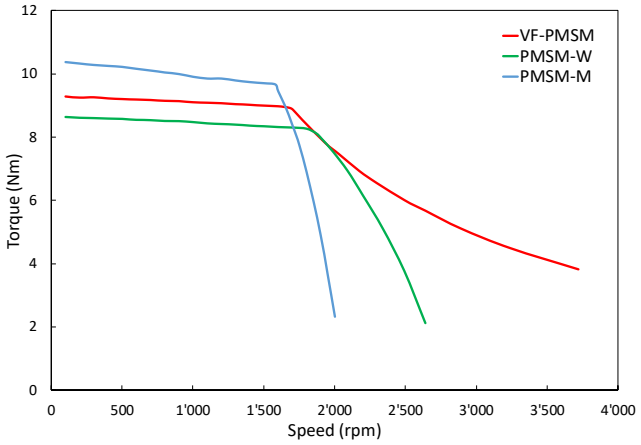

Fig. 13 Measured torque-speed characteristics of PMSM under nominal current (VDC = 600 V)

The conventional approach of flux-weakening enhanced the speed of M-type and W-type at the expense of a significant drop of torque and efficiency, due to the lack of available current to generate the torque. As reported in Table IV, the approach for the VF-PMSM has substantially enhanced the operating speed. In steady-state, the current is fully dedicated for the torque, which justifies a greater torque in the area of HS-LT operation.

TABLE IV
Measured Torque (Nm) at Different Operating Points

	Speed (rpm)				Current (A) at 100 (rpm)	
	1500	2000	2640	3720	3.0	12.0
PMSM-M	9.7	2.3	-	-	10.2	38.9
PMSM-W	8.3	7.5	2.1	-	8.5	34.3
VF-PMSM	9.17	7.6	5.7	3.8	9.2	33.9

Fig. 14 presents the mechanical power-speed characteristic for I=3 A_{rms}. For this nominal current, the output power falls abruptly when the standard flux-weakening process is applied to increase the speed beyond its nominal value. The method of MS manipulation keeps the mechanical power significantly constant due to the absence of the current i_d.

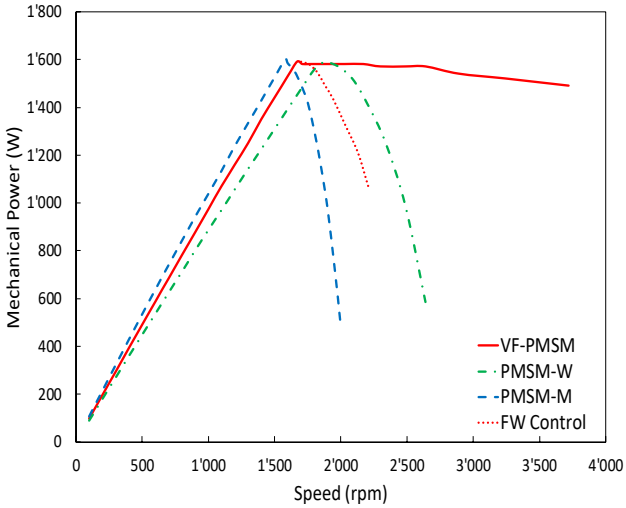

Fig. 14 Measured mechanical power of PMSM

The performance of VF-PMSM in the HS-LT operating zone is explained by a current fully dedicated for the torque and limited iron losses.

The classical flux weakening method was also applied on the VF-PMSM, represented with the dotted curve in Fig. 14, by limiting i_d up to 0.8 pu to prevent any change of the rotor MS. A measurement of no-load back-emf allowed verifying that the magnetization has not been modified.

Fig. 15 presents the torque-current characteristics of the motors operating at 100 rpm. It emphasizes a characteristic of VF-PMSM similar to the PM motors, even when current reaches 4 pu, despite a slight magnetic saturation.

A test under nominal conditions, according to the standard IEC 60034-30-2, shows that the motors are all classified as IE5.

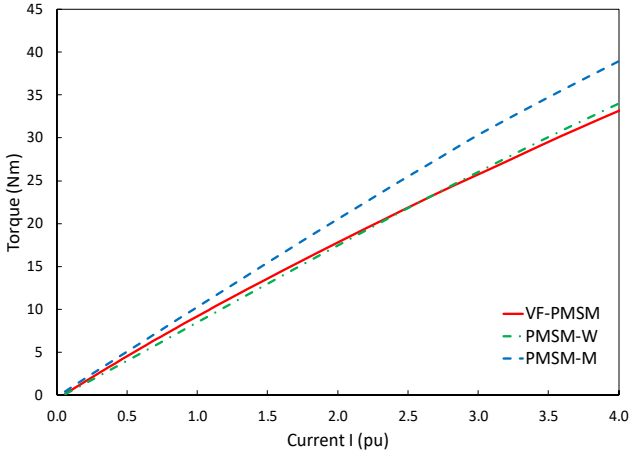

Fig. 15 Comparison of measured characteristics torque-current at 100 rpm

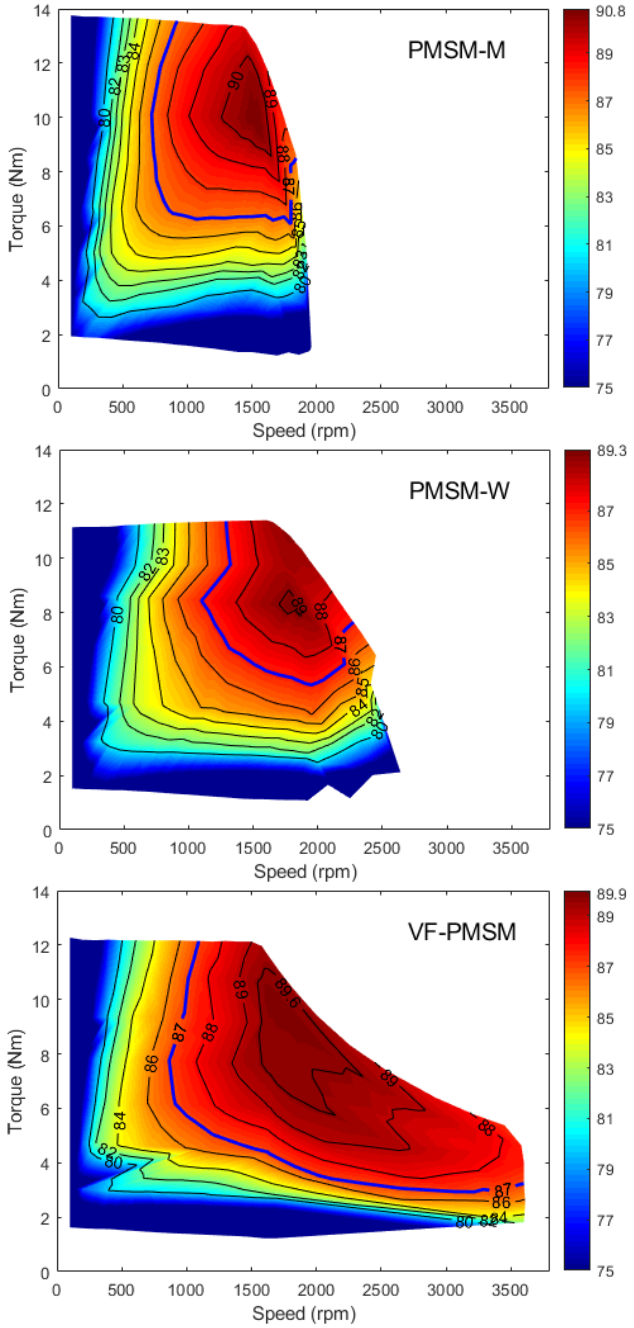

Fig. 16 Measured efficiency map for PMSM-M, PMSM-W and VF-PMSM (I ≤ 4Arms)

Fig. 16 displays the efficiency map of each motor considered in this paper under a current lower than 4 A_{rms}. The map of VF-PMSM is a superposition of measured characteristics for different MS level. Only the optimal efficiency is represented for an operating point where different rotor MS is possible. An area, where efficiency greater than 87% is delimited, emphasizes the flexibility of operation. Therefore, the MS manipulation gives an additional degree of freedom to VF-PMSM over conventional PMSMs, and this freedom can be used to minimize the losses and optimize the efficiency according to the load conditions. In addition, it is interesting to mention that a potential damaging overvoltage can occur with a standard permanent magnet synchronous motor, due to the interruption of flux weakening. This risk is reduced with the VF-PMSM since the excitation flux is first lowered before the increase of speed.

To complete the comparison of PM motors, the M-type motor has a mass of NdFeB magnets 48% greater than the W-type, which partly explains the measured performances for both motors. The VF-PMSM and the W-type motor have the same mass of NdFeB in the rotor. The additional use of AlNiCo in the VF-PMSM increases the total mass of magnets by 88%, compared to the W-type motor. However, the cost of AlNiCo, which is significantly cheaper than NdFeB, and the typical rectangular dimension of the manufacturer, allows the VF-PMSM to stay competitive against the M-type, in terms of cost for magnets in a production over 1000 units.

Fig. 17 Manufacture version of VF-PMSM rotor

VI. Summary

VF-PMSM, also called the Memory motor, can modify the excitation flux generated by its permanent magnets using short current pulses applied in the d-axis. The combination of magnets with different coercive forces leads to create an equivalent magnetic field crossing the air gap, which can be strengthened or weakened by changing the magnet polarity of AlNiCo. The operation of the VF-PMSM is identical to conventional PM motors, including a standard field-oriented control that only provides some pulses to change the motor constants (K_E/K_T). Based on this knowledge, a prototype was developed, which is used to evaluate its performance against two PMSMs typical of those found among manufacturers. The tests were carried out using the same stator and winding, in the same conditions, making the comparison of rotors possible. It emphasized the capability of the VF-PMSM to be used in wide speed applications, since it is equivalent to combine several PM motors into one, which offers a degree of freedom to optimize the efficiency.

These results motivated the development of a new design for VF-PMSM. This version presents an interior permanent magnet (IPM) with features similar to the prototype in Fig. 5, made of stacks of thin sheets that can be cheap and easily manufactured. The structure of the salient pole rotor includes several slots where magnets can be slipped in, as seen in Fig. 17. Note that, other than the design of the rotor, the entire equipment used in this paper was conventional, including the inverter and the field-oriented vector control with an adapted strategy for the pulses.

VII. Conclusion

In many applications of PMSMs using a conventional flux weakening control, such as electric vehicles, the VF-PMSM could be a competitor to improve performance and efficiency. This paper has emphasized that the investment cost of MS manipulations (energy of pulses, inverter sizes and capabilities) can be compensated by the performance and the flexibility compared to conventional PMSMs. Furthermore, the proposed approach in this paper let us carry out a comparison that is strictly focused on the performance of the rotors. Experimental results have pointed out some highlights such as:

- The ability to expand the operating range of the torque-speed characteristic with high efficiency, thanks to a sustainable and permanent adjustment of excitation flux via short current pulses i_d.
- The energy cost during a pulse of the magnetization or demagnetization phase is negligible compared to a steady-state operation.
- A current i_q, which can be the same order of magnitude as i_d pulses, can generate a torque without changing the rotor MS.
- The VF-PMSM can be fully manufactured as an IPM motor.
- Control strategies can be adapted and optimized to exploit the special properties of these machines in order to minimize losses for the torque and speed operating point. Assuming two operating modes, the vector control can already efficiently exploit the VF-PMSM. A suitable control strategy may be required if current pulses are frequently applied to optimize every operating point.

Acknowledgment

The authors wish to thank LANDERT MOTOREN AG, Samuel Chevailler from HES-SO Sion, Luc Bossoney and Marc-André Pointet from HES-SO Yverdon-les-Bains, for their contribution.

References

[1] R. Owen, Z. Q. Zhu, J. B. Wang, D. A. Stone, and I. Urquhart, "Review of variable-flux permanent magnet machines," *in International Conference on Electrical Machines and Systems,* 2011, pp. 1–6.

[2] A. Toba, A. Daikoku, N. Nishiyama, Y. Yoshikawa, and Y. Kawazoe, "Recent technical trends in variable flux motors," *in International Power Electronics Conference (IPEC-Hiroshima - ECCE ASIA),* 2014, pp. 2011–2018.

[3] H. Jia, W. Xinjian, and S. Zechang, "Variable flux memory motors: A review," *in IEEE Conference and Expo Transportation Electrification Asia-Pacific (ITEC Asia-Pacific),* 2014, pp. 1–6

[4] V. Ostovic, "Memory motors-a new class of controllable flux PM machines for a true wide speed operation," *in Conference Record of the IEEE Industry Applications Conference. 36th IAS Annual Meeting (Cat. No.01CH37248),* 2001, vol. 4, pp. 2577–2584.

[5] C. Yiguang, P. Wei, W. Ying, T. Renyuan, and W. Jing, "Interior composite-rotor controllable-flux PMSM - memory motor," *in International Conference on Electrical Machines and Systems,* 2005, vol. 1, p. 446–449.

[6] K. Sakai, K. Yuki, Y. Hashiba, N. Takahashi, and K. Yasui, "Principle of the variable-magnetic-force memory motor," in *International Conference on Electrical Machines and Systems,* 2009, pp. 1–6.

[7] C. Besson, A. Savary, and M. Jaccard, "Brushless permanent-magnet synchronous motor with magnetization and demagnetization of magnets during operation," *ELECTROMOTION*, no. 22, pp. 3–13, Jan. 2015.

[8] D. Wu, Z. Q. Zhu, X. Liu, A. Pride, R. Deodhar, and T. Sasaki, "Cross coupling effect in hybrid magnet memory motor," *in 7th IET International Conference on Power Electronics, Machines and Drives,* 2014, pp. 1–6.

[9] Y. Zhou, W. Wang, and Y. Chen, "Design and analysis of a novel hybrid permanent magnet memory motor," in *17th International Conference on Electrical Machines and Systems (ICEMS)*, 2014, pp. 2687–2692.

[10] A. Athavale, K. Sasaki, B. S. Gagas, T. Kato, and R. D. Lorenz, "Variable flux permanent magnet synchronous machine (VF-PMSM) design to meet electric vehicle traction requirements with reduced losses," *in IEEE Energy Conversion Congress and Exposition (ECCE),* 2016, pp. 1–8.

[11] A. Sun, J. Li, R. Qu, J. Chen, and H. Lu, "Rotor design considerations for a variable-flux flux-intensifying interior permanent magnet machine with improved torque quality and reduced magnetization current," *in IEEE Energy Conversion Congress and Exposition (ECCE),* 2015, pp. 784–790.

[12] M. Ibrahim, L. Masisi, and P. Pillay, "Design of Variable-Flux Permanent-Magnet Machines Using Alnico Magnets," *IEEE Trans. Ind. Appl.*, vol. 51, no. 6, pp. 4482–4491, Nov. 2015.

[13] N. Limsuwan, T. Kato, K. Akatsu, and R. D. Lorenz, "Design and Evaluation of a Variable-Flux Flux-Intensifying Interior Permanent-Magnet Machine," *IEEE Trans. Ind. Appl.,* vol. 50, no. 2, pp. 1015–1024, Mar. 2014.

[14] C. Yu, K. T. Chau, and J. Z. Jiang, "A permanent-magnet flux-mnemonic integrated-starter-generator for hybrid electric vehicles," *in IEEE Vehicle Power and Propulsion Conference*, 2008, pp. 1–6.

[15] J. M. Kim, J. Y. Choi, K. S. Lee, and S. H. Lee, "Design and Analysis of Surface-Mounted-Type Variable Flux Permanent Magnet Motor for Wide-Speed Range Applications," *IEEE Trans. Magn.,* vol. 51, no. 11, pp. 1–4, Nov. 2015.

[16] A. Athavale, B. S. Gagas, R. D. Lorenz, K. Sasaki, and T. Kato, "Effect of dynamic magnetization manipulation on transient losses and magnet temperature in energy-saving VF-PMSM traction drives," *in 19th European Conference on Power Electronics and Applications (EPE'17 ECCE Europe),* 2017, p. P.1-P.10.